Journal of Molecular Catalysis A: Chemical 335 (2011) 97–104

Contents lists available at ScienceDirect

Journal of Molecular Catalysis A: Chemical

journal homepage: www.elsevier.com/locate/molcata

Alkoxyl-derived visible light activity of TiO_2 synthesized at low temperature

Jingjing Jiang, Mingce Long*, Deyong Wu, Weimin Cai**

School of Environmental Science and Engineering, Shanghai Jiao Tong University, Dong Chuan Road 800, Shanghai 200240, China

ARTICLE INFO

Article history:
Received 25 September 2010
Received in revised form
11 November 2010
Accepted 12 November 2010
Available online 21 November 2010

Keywords:
Visible light activity
Low temperature
Surface states

ABSTRACT

A visible-light responsive anatase TiO_2 was synthesized with a facile peptization-reflux method at 120 °C, using tetrabutyl titanate (TBT) as the titanium precursor. According to the results of various experiments and characterizations, we observed that in the low-temperature synthetic process of TiO_2 catalysts, there is an equilibrium of hydrolytic decomposition and re-combination of Ti–(O–R) bond from the titanium precursor; the presence of acid and hydrolysis products (*n*-butanol) cooperatively lead to the retention of more alkoxyl groups on the anatase surface. Upon visible light irradiation, excited electrons could be generated from these alkoxyl-derived surface states, and the photocatalytic reactions through a ligand-to-metal charge transfer (LMCT) process were thus initiated.

1. Introduction

Titanium dioxide has been widely used in photo-assisted degradation and mineralization of organic contaminants because of its excellent property (such as non-toxicity, good stability and low material cost); however, it can utilize only a small UV part (about 3–5%) of solar light owning to its wide band gap (anatase, E_{bg} = ca. 3.2 eV; rutile, E_{bg} = ca. 3.0 eV) [1–4]. Therefore, a remarkable effort has been made in recent years to obtain visible-light-activated TiO_2-based materials by cations doping [5–9] (such as Fe^{3+}, Cr^{3+}, Co^{2+}, V^{4+}, Mo^{5+}, Ru^{3+}), anions doping [10–14] (such as N, S, C, I, P, F, B), or co-doping with several ions.

The methods of ion doping always need expensive apparatus, or high-temperature treatment process (often > 300 °C) for the implantation of external atoms. In consideration of energy saving and wider usage, many works have been done to develop simple and low-temperature methods of ion doping based on hydrothermal treatments, or some modified sol–gel methods [15–20]. In the reports of these works, authors always focused on the discussion of activity promotion caused by the doped ion; however, seeing the data from these reports, we discovered another fact that while $Ti(OBu)_4$ is used as the titanium precursor, some "undoped" TiO_2 prepared at a low temperature could achieve a much better photocatalytic activity than Degussa P25 under solar light, which is always explained as the effect of enhanced adsorption rate caused by smaller particle size [17–20].

However, from the results of our experiments, the reason for this interesting phenomenon seems not to be so simple. In the process to synthesize nitrogen-doped TiO_2 with $Ti(OBu)_4$ as the titanium precursor, we are surprised to find that the "undoped" titania, which is prepared as a control, exhibits a visible-light activity just a little worse than the doped ones. Similarly, in the report of Hao et al. [21], the undoped TiO_2 crystallized by refluxing also shows a good photocatalytic activity under visible light (λ > 420 nm), which has not been emphasized by the author. Although the catalyst particle size is a crucial factor in the heterogeneous photocatalysis [22], a smaller particle size of titania is not sufficient for inducing an increased visible-light activity [23–26]. In this paper, we try to describe the main reason for the promoted visible-light activity of these "undoped" catalysts. It is shown, that the retention of superficial alkoxyl groups in the synthetic process could lead to an effective visible-light activity. Mechanism for the visible-light induced catalytic process on this alkoxyl-derived surface modified titania has also been tentatively discussed.

2. Experimental

2.1. Sample preparation

The catalyst powder was simply prepared by controlled hydrolysis of tetrabutyl titanate (TBT) in nitric acid solution at room temperature (about 15 °C), followed with a crystalling process. 5 ml tetrabutyl titanate (>98%, Shanghai Reagent Co. Ltd., China) was added dropwise into nitric acid solution under vigorous stirring to yield a molar concentration of H^+ in the starting mixture of 0.2 M (H^+/Ti about 0.5, total volume about 40 ml). After several hours, a light yellow sol was formed. After ageing the sol for 12 h under

* Corresponding author. Tel.: +86 21 54747354; fax: +86 21 54740825.
** Corresponding author. Tel.: +86 21 54748019; fax: +86 21 54748019.
E-mail addresses: long_mc@sjtu.edu.cn (M. Long), wmcai@sjtu.edu.cn (W. Cai).

1381-1169/$ – see front matter © 2010 Elsevier B.V. All rights reserved.
doi:10.1016/j.molcata.2010.11.019

continuous stirring at room temperature, it was further treated in the following three ways:

(1) *Direct drying*: The as-prepared sol was directly dried at 80 °C in oven, ground in an agate mortar and washed for several times to thoroughly remove the adsorbed hydrogen ions. After drying, a fine yellow catalyst powder was achieved, named H-80.
(2) *Reflux*: The sol was treated under refluxing at 120 °C. Continuous stirring and sufficient condensation were essential to keep the sol from coagulation. After 12 h, the sol turned out to be a homogeneous, white emulsion. The emulsion was then dried at 80 °C in oven, ground and washed for several times; the as-prepared yellow powder was named RH-80.
(3) *Hydrothermal treatment*: The sol was treated in autoclave at 120 °C, with filling degree of about 80%. After 12 h, a light yellow precipitation was formed. The precipitation was dried in oven (80 °C) with the whole solution, ground and washed for several times; the as-prepared yellow powder was named AH-80.

2.2. Characterization

X-ray diffraction analysis (XRD) was carried out using a Rigaku D/Max2200/PC X-ray diffractometer with Cu K_α radiation at 40 kV and 20 mA, and the diffraction angle 2θ was scanned in 20–80° with step of 0.02°. HRTEM images of samples were obtained on a JEM-2100F Transmission Electron Microscope. X-ray photoelectron spectroscopy (XPS) measurements were performed on a RBD upgraded PHI-5000C ESCA system (Perkin Elmer). UV–vis diffuse reflectance spectra (DRS) were recorded on a TU-1901 UV/vis spectrophotometer (Beijing purkinje general instrument Co., Ltd., China). The conversion from reflection to absorption was conducted by the Kubelka–Munk method, and the indirect band-gap energies of investigated samples were estimated by the intercept of the tangent in the plots of $(\alpha h\nu)^{1/2}$ vs. photon energy ($h\nu$). Fourier transform infrared spectroscopy (FTIR) was performed at a scanning range of 4000–370 cm^{-1} on an EQUINOX-55 Infrared-Raman Spectroscope (Bruker Co., Germany) with DTGS detector. Carbon contents of samples were studied by PE-2400 II CHNS/O Analyzer (Perkin Elmer Co., America).

2.3. Photocatalytic reaction and photoelectrochemical test

The optical system for photocatalytic reaction consists of a 1000 W xenon lamp and a cutoff filter (λ > 400 nm). In a typical photocatalytic activity test, 0.05 g catalyst was added into 50 ml methyl orange (MO) solution (10 mg/L), stirred in dark for 30 min to reach an adsorption equilibrium before irradiation. There was little pH change of MO after the addition of catalysts, and the temperature for photocatalytic reaction was maintained at about 15 °C by cooling water. Under continuous stirring, samples were taken at every time intervals (30 min) and centrifuged for the removal of photocatalysts. Concentration of the filtrate was analyzed by a UNICO UV-2102 spectrometer at 464 nm.

Photoelectrochemical test systems were composed of a CHI 600D Electrochemistry potentiostat, a 500 W Xenon lamp with or without cutoff filters (λ > 420 nm) and a homemade three electrode cell (a platinum wire as counter electrode, Ag/AgCl as reference electrode and Na_2SO_4 (0.5 M) as electrolyte). Working electrode was prepared by depositing the suspension of the catalyst powder (0.1 g sample dispersed in 1 ml deionized water) onto a fluorine-doped tin oxide-coated glass with doctor-blade coating method. During measurements, the electrode was pressed against an O-ring of an electrochemical cell, with a working area of about 0.78 cm^2.

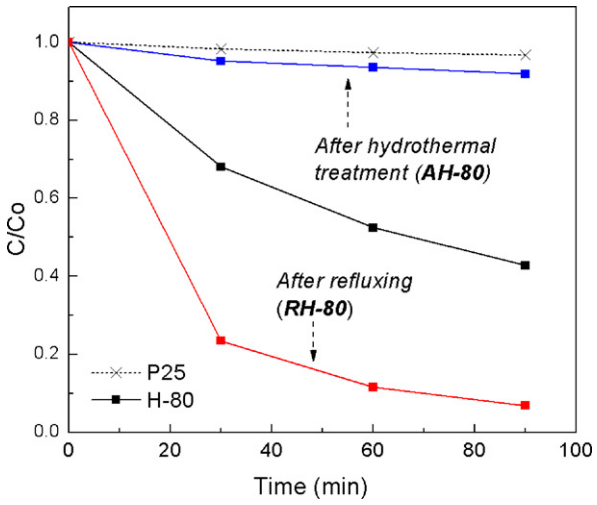

Fig. 1. Photodegradation of MO on different TiO_2 samples under visible light (λ > 400 nm).

3. Results and discussion

3.1. Photocatalytic activity

Fig. 1 shows the photocatalytic activity of the as-prepared three samples in the degradation of MO, using Degussa P25 as a control. As can be seen from the curve, Degussa P25 shows very little photoactivity under visible light, which indicates that the degradation of MO by dye sensitization is negligible. Noticeably, the powder prepared by direct drying of the aged-sol (H-80) achieves an appreciable degradation rate of MO. However, after hydrothermal treatment of the sol for another 12 h, the visible light activity of the as-prepared powder (AH-80) decreased greatly. Contrary to that, the powder obtained after further refluxing (RH-80) exhibits a good increase of its activity: in the presence of RH-80, more than 90% of MO is degraded within 90 min under visible light irradiation, which is much better than H-80 (57.3%) and AH-80 (<10%).

Measurements of the photoelectrochemical properties on sample RH-80 and AH-80 were also conducted to confirm their difference in the visible-light response. In the cyclic voltammetry (CV) curve of the two samples (shown in Fig. 2), no obvious peaks

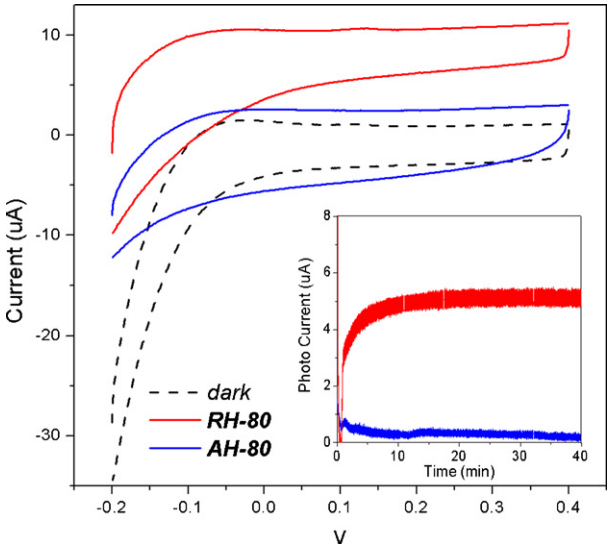

Fig. 2. Cyclic voltammetry curves on the RH-80 and AH-80 electrode, with photocurrent test (λ > 420 nm) at 0 V bias vs. Ag/AgCl (inset).

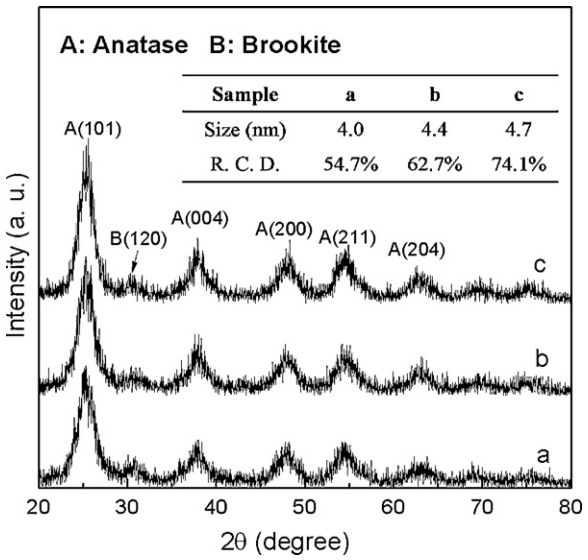

Fig. 3. XRD patterns of different TiO_2 samples (a) H-80, (b) RH-80 and (c) AH-80 (inset: estimated particle size and relative crystalline degree of each sample).

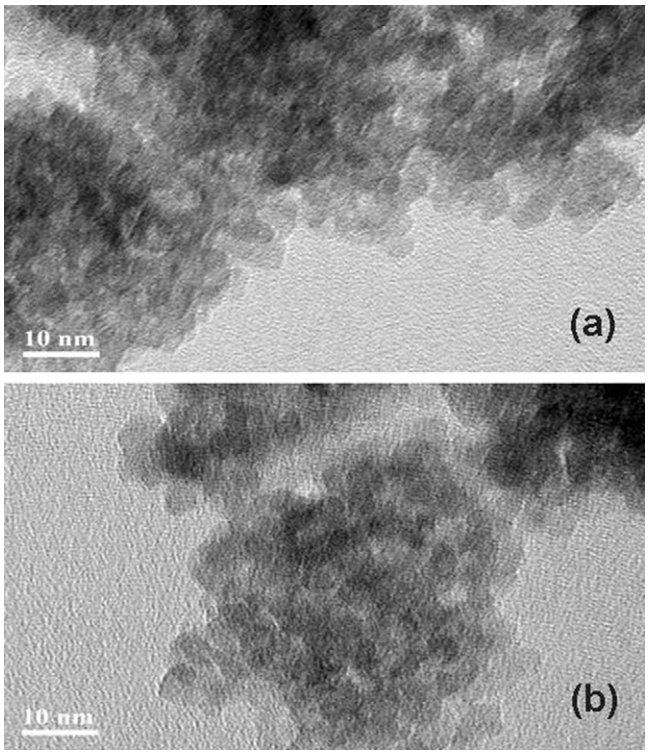

Fig. 4. TEM images of sample RH-80 (a) and AH-80 (b).

were observed both in the dark and under visible light ($\lambda > 420$ nm), indicating the absence of any oxidation or reduction processes occurred during the change of external bias. On the RH-80 electrode, the visible-light irradiation has induced an obvious current increase under bias from −0.2 to 0.4 V (vs. Ag/AgCl), which is hard to be detected on the AH-80 electrode. Moreover, there is an obvious visible-light-induced photocurrent on the RH-80 electrode at 0 V bias (inset of Fig. 2), while on the AH-80 electrode, the photocurrent is indeed slight. The big contrasts both on the value of visible-light induced photocurrent and the visible-light degradation rate of MO fully revealed the intrinsic property differences between RH-80 and AH-80.

As is stated above, the synthetic processes of AH-80 and RH-80 are kept almost the same except for the crystallizing method. Therefore, the difference of their visible-light activity should not be caused by the impurities that may exist in the raw materials. Nevertheless, there must be some critical changes in the refluxing process that could make an improvement of the visible-light activity of the final titania, which are not favored in the autoclave.

3.2. Evidence of the alkoxyl-derived visible light activity

3.2.1. Search for the origin of visible-light activity

Since the crystal form and particle size are important factors for heterogeneous catalysts, the X-ray diffraction patterns and HRTEM images of the as-prepared TiO_2 samples were both obtained; the results are shown in Figs. 3 and 4, respectively. As can be seen from Fig. 3, all the samples were mainly anatase with a trace of brookite. The particle size in the inset table is calculated by the *Debye–Scherer* formula, and the relative crystalline degree (R.C.D.) is denoted by the relative peak height of anatase (1 0 1) plane comparing to the TiO_2 sample calcined at 400 °C. From the data of the table, we observed that the sample RH-80 and AH-80 both revealed a slight increase in the particle size, as well as the crystallity of anatase in comparison to the H-80 powder. From the TEM images of sample RH-80 and AH-80 (Fig. 4), we can see that both samples are consisted of the spherical-shaped nanoparticles, and the average particle size of sample RH-80 and AH-80 are estimated as 4.3 nm and 4.8 nm, respectively, which is in good correspondence to the value calculated from the XRD patterns. Since there are no obvious differences between sample RH-80 and AH-80 either in the crystal form or morphology, and the visible-light activities of sample H-80, RH-80 and AH-80 are not corresponding to their particle sizes (the H-80 powder, which possesses the smallest particle size among the three samples, is not the one whose visible-light activity is the highest), there must be another factor that could really contribute to the observed visible-light activity.

In the FTIR spectra (Fig. 5) of sample H-80, RH-80 and AH-80, however, there appeared some remarkable differences. The diffused band between 1740 and 3625 cm^{-1}, centering about 3420 cm^{-1} is ascribed to the O–H stretching of surface hydroxyl groups, as well as the molecularly adsorbed water [27]; the band around 1625 cm^{-1} is caused by the O–H bending vibrations [28]. Noticeably, despite the great influence of O–H stretching absorptions, there are still two detective bands at 2924 and 2852 cm^{-1} (Region 1, shown in Fig. 5) which represents for the stretching vibrations of $–CH_2–$ groups [29]. Moreover, in another region between 1515 and 1200 cm^{-1} (Region 2), the diffused absorption on sample AH-80 generally involves the stretching vibration of –C–O– (1265 cm^{-1}) [30], bending vibration of $–CH_3$ (1380 cm^{-1}) [31], and in-plane deformation vibration of H atom in the CO–H group (1410 cm^{-1}) [32]. However, for samples of H-80 and RH-80, the absorption band from CO–H vibration (1410 cm^{-1}) is harder to be detected, while the absorption of $–CH_3$ vibration (1380 cm^{-1}), which is indeed slight in the AH-80 powder, becomes much more obvious. According to these results, we assumed that during the high-pressure synthetic process of AH-80, some of the *n*-butanol molecules, the hydrolysis products of TBT, could be linked on the titania surface by BuOH···HO–Ti binding, and mostly stated in an associated form. Since the slight H-bond interactions in the form of CH···O binding could lead to a shortened C–H bond [33–35], the bending vibrations of $–CH_2–$ and $–CH_3$ groups on sample AH-80 are really ambiguous. However, for samples of H-80 and RH-80, the alkyl groups may exist in the form of Bu–O–Ti binding (alkoxyl group). As a result, the vibration of terminal $–CH_3$ groups could hardly be affected by H-bond interactions because they are simply too far away from the surface Ti–OH groups.

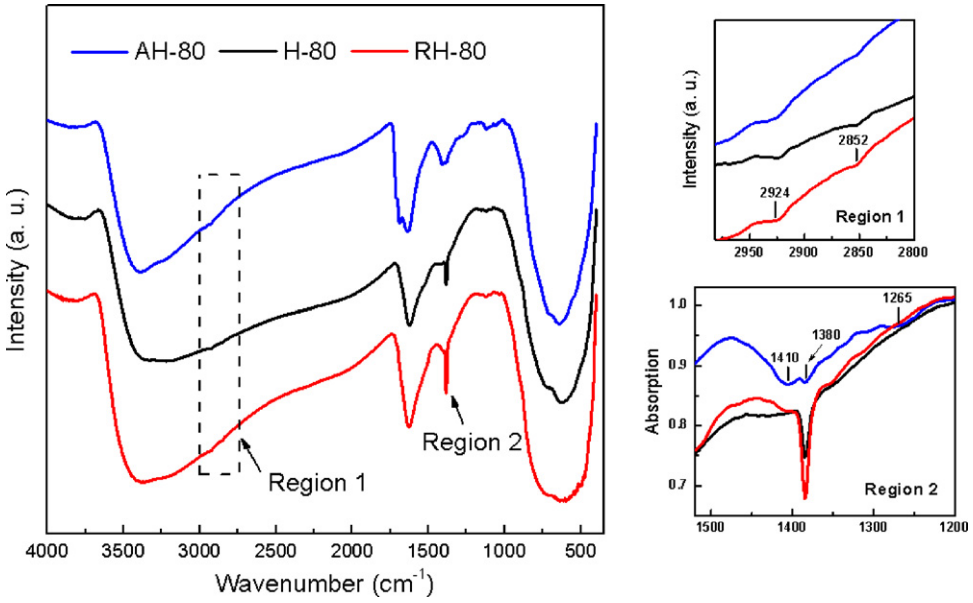

Fig. 5. IR spectra of different TiO_2 samples, with two magnified regions at: (I) 2980–2800 cm^{-1}, (II) 1515–1200 cm^{-1}.

There is another important fact, that the intensity of the absorption peak at 1380 cm^{-1}, which is considered to be the sign of alkoxyl groups, has achieved a good correspondence to the visible-light degradation efficiency of MO (RH-80 > H-80 > AH-80, shown in Fig. 5). To confirm this phenomenon, we conducted a post heat treatment on sample RH-80, which possesses the most amounts of alkoxyl groups. The temperature in muffle furnace was raised up to 240 °C and 300 °C with a heating rate of 10 K/min and kept for 3 h. The as-prepared TiO_2 samples were named RH-240 and RH-300, respectively. As shown in Fig. 6, with the increase of calcination temperature, the RH-80 powder underwent a color change from light yellow to dark brown (RH-240), and then almost white (RH-300), which is always observed in the heat treatment of carbon-containing TiO_2 samples [24–26]. From the results of photocatalytic activity tests (Fig. 6), we observed a decrease of MO degradation efficiency as the temperature increases; correspondingly, in the IR spectrum (Fig. 7), the absorption peak at 1380 cm^{-1} also decreased with the increasing temperature. Therefore, we considered that the alkoxyl groups on sample H-80 and RH-80 may have played an important part in the visible-light catalytic process.

3.2.2. *Further confirmation of the visible-light active alkoxyl groups*

Previously we discovered the different amount of alkoxyl groups on samples with different visible-light activity, and the removal of alkoxyl linkages on sample RH-80 after heat treatment also induced an obvious decrease of its activity. However, it remains unclear if the newly formed alkoxyl groups on the titania surface could lead to a better visible-light activity. To search for the answer to this question, a series of catalysts were prepared through the variation of two important factors in the refluxing process: (I) nitric acid; (II) the hydrolysis product of TBT–*n*-butanol. Detailed methods are shown in Table 1, and comparisons of the visible-light activity for different samples are shown in Table 2.

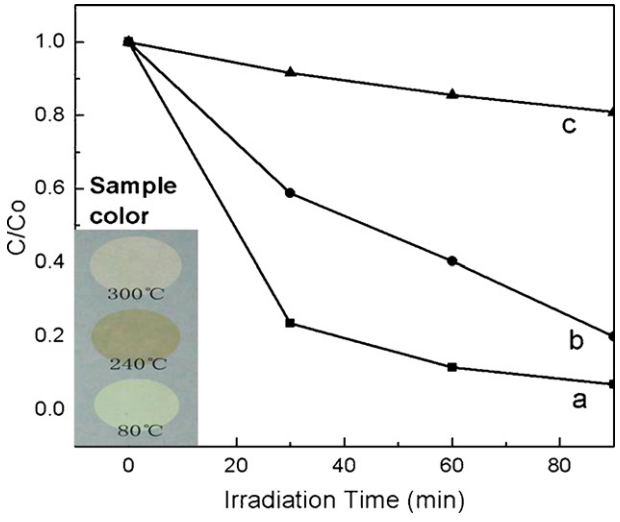

Fig. 6. Visible light degradation of MO on TiO_2 samples (a) RH-80, (b) RH-240, (c) RH-300 (with the photos of sample color) (For interpretation of the references to color in this figure legend, the reader is referred to the web version of the article.).

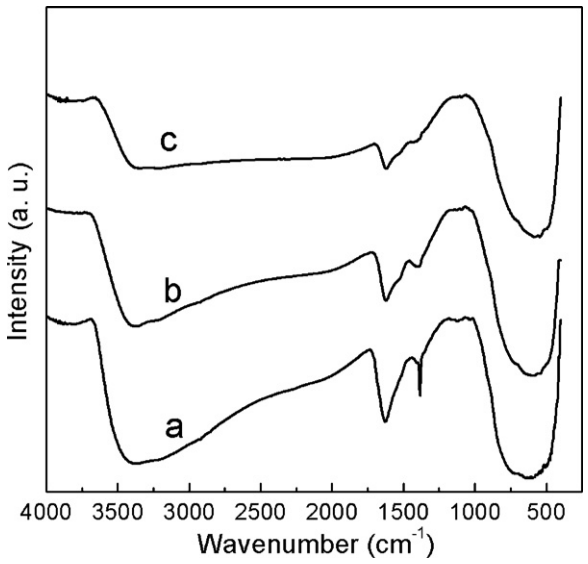

Fig. 7. IR spectra of different TiO_2 samples (a) RH-80, (b) RH-240 and (c) RH-300.

Table 1
Synthetic methods for different TiO_2 samples[a].

Sample	Synthetic methods (total volume = 40 ml)		H^+/Ti
	Step 1 (room temperature)	Step 2 (120 °C, 12 h)	
H-80	5 ml TBT added dropwise into HNO_3 solution, stirred for 12 h	–	0.5
RH-80		Reflux	0.5
AH-80		Hydrothermally treated in autoclave	0.5
R-80	5 ml TBT added dropwise into DI water, stirred for 12 h	Reflux	0
P100	5 ml TBT added dropwise into DI water, stirred for 12 h, and the precipitation was washed several times for alcohol removal before further treatment	Dispersed in DI water, reflux	0
PH100		Dispersed in HNO_3 solution, reflux	0.5
P102		Dispersed in aqueous solution with butanol (*n*BuOH:*n*Ti = 2:1), reflux	0
PH101, 102,104		Dispersed in HNO_3 solution, added with different dosage of *n*-butanol (*n*BuOH:*n*Ti = 1:1, 2:1, 4:1), reflux	0.5

[a] After Step 2, the post treatment of the as-prepared suspension (or sol) is the same as that of H-80 for each sample.

The data shown in Table 2 reveals the synergistic effect of nitric acid and *n*-butanol. In the perspective of nitric acid, we observed that no matter the hydrolysis product (*n*-butanol) is removed or not, the participation of acid in the synthetic process could lead to a great increase of the MO degradation efficiency for the final catalysts (PH100 > P100, RH-80 > R-80 and PH102 > P102). In the perspective of hydrolysis product, we can see that in the absence of acid, the powder synthesized by alcohol-free method (P100) obtains a lower visible-light activity than that synthesized with alcohol (R-80). However, while the *n*-butanol is re-added to the alcohol-free suspension before Step 2, the final power reaches a recovery of its activity (P102). In the presence of acid, the effect of *n*-butanol is much more obvious: the powder refluxed with the presence of *n*-butanol at low pH (PH102) obtains a MO degradation rate of 77.0% under visible light irradiation after 90 min, compared to only 33.0% of the powder prepared without butanol (PH100).

In Fig. 8A, we discovered that during the synthetic process, the single addition of acid (PH100) or *n*-butanol (P102) before Step 2 could not lead to an obvious alkoxyl vibration in the IR spectrum; however, while they are both added (PH102), the alkoxyl vibration is much more obvious. From the XRD patterns, the particle sizes of sample PH100, P102 and PH102 were calculated as 3.9, 5.4 and 4.3 nm, respectively, which revealed no correspondence to their visible-light activities. However, comparing the experimental results shown in Fig. 8A and B, we discovered a good correlation between the MO-degradation efficiency and the amount of alkoxyl groups formed in the refluxing process, as well as the total content of carbon contained in the TiO_2 sample (RH-80 > PH102 > PH100).

From the XPS analysis of sample RH-80 and PH104, the Ti 2p region (Fig. 9a) revealed two peaks around 458.2 and 463.6 eV, which represents for the binding energy of Ti 2p3/2 and Ti 2p1/2, respectively; in O 1s region (Fig. 9b), the peak located at 529.6 eV is attributed to the lattice oxygen, while another peak at about 531.6 eV is sourced from the surface Ti–OH groups. More importantly, in the C1 s region (Fig. 9c), despite the first two peaks (around 284 and 285.5 eV) from adventitious elemental carbons [36], the binding energy around 288 eV suggests the presence of Ti–O–C bond [15], which is a strong evidence for the presence of alkoxyl groups on sample RH-80 and PH104. However, the Ti–O–C peak observed on PH104 is weaker than that on RH-80, which indicates the less amount of (Ti–O)–R bonds possessed by PH104.

To get a further confirmation of the alkoxyl-derived visible light activity, samples of Degussa P25 and AH-80, which had exhibited little visible-light activity, were further treated by refluxing with the presence of acid and *n*-butanol (similar to the synthetic process of PH104 in Step 2). From Fig. 10, we can see that after refluxing, an increase of the visible-light activity was observed both on AH-80 and Degussa P25. Considering the greater activity increase observed on AH-80, we supposed that during the refluxing process, the level of alkoxyl re-formation was greatly dependent on the surface property and crystallization degree of the initial titania. Furthermore, both the XRD and IR tests revealed no obvious changes on sample AH-80 and Degussa P25 after refluxing, which could be understood by the especially low amount of newly formed alkoxyl linkages on these well-crystallized titania surfaces.

Table 2
Effects of considered factors in the synthetic process.

Considered factors		Sample	Simplified method	Photodegradation of MO	
				R[d]	*k*[e]
I. Nitric acid (0.2 M)	Without alcohol: effect of acid	PH100	A[a] + H^+; reflux	0.330	4.16E−03
		P100	A; reflux	0.170	2.01E−03
	With alcohol: effect of acid added before Step 1	RH-80	Sol; reflux	0.931	1.86E−02
		R-80	B[b]; reflux	0.397	5.16E−03
	With alcohol: effect of acid added before Step 2	PH102	A + H^+ + 2:1 BuOH[c]; reflux	0.766	1.27E−02
		P102	A + 2:1 BuOH; reflux	0.421	5.54E−03
II. Hydrolysis product (*n*-butanol)	Without acid: effect of alcohol	R-80	B; reflux	0.397	5.16E−03
		P100	A; reflux	0.170	2.01E−03
		P102	A + 2:1 BuOH; reflux	0.421	5.54E−03
	With acid: effect of alcohol added before Step 2	PH100	A + H^+; reflux	0.330	4.16E−03
		PH102	A + H^+ + 2:1 BuOH; reflux	0.766	1.27E−02
	With acid: effect of alcohol added before Step 2 with different dosage	PH101	A + H^+ + 1:1 BuOH; reflux	0.725	1.16E−02
		PH102	A + H^+ + 2:1 BuOH; reflux	0.766	1.27E−02
		PH104	B + H^+ + 4:1 BuOH; reflux	0.770	1.29E−02

[a] Suspension made by dispersing the alcohol-free precipitation into DI water.
[b] Suspension produced by hydrolysis of TBT in the absence of acid (with alcohol).
[c] The molar ratio of BuOH to Ti is 2:1.
[d] Removal efficiency of MO (10 mg/L) after 90 min.
[e] The photodegradation process accords with the first order reaction kinetics, and the kinetic constants for different samples are shown in the table (min^{-1}).

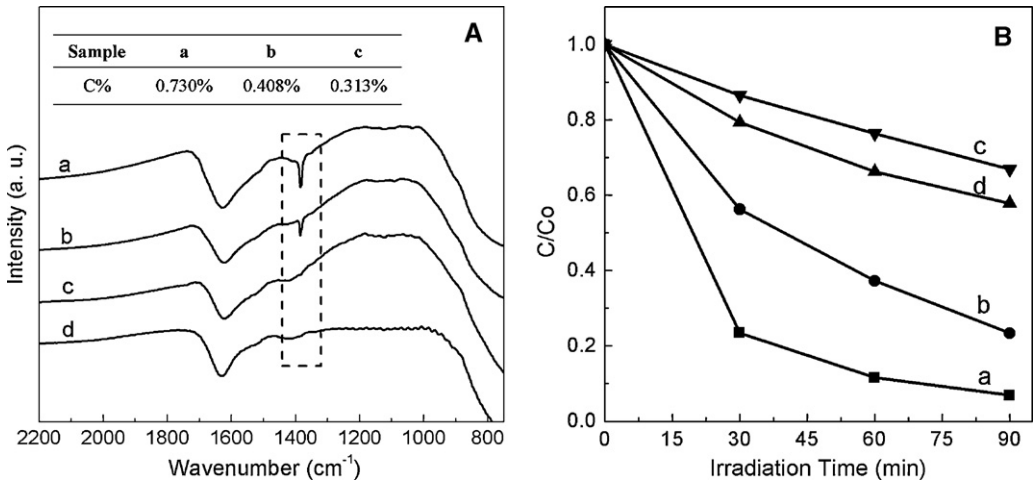

Fig. 8. Different property of TiO_2 samples synthesized with different methods (a) RH-80, (b) PH102, (c) PH100 and (d) P102. (A) The IR spectra (inset: carbon content of sample RH-80, PH102 and PH100); (B) the degradation of MO under visible light irradiation ($\lambda > 400$ nm).

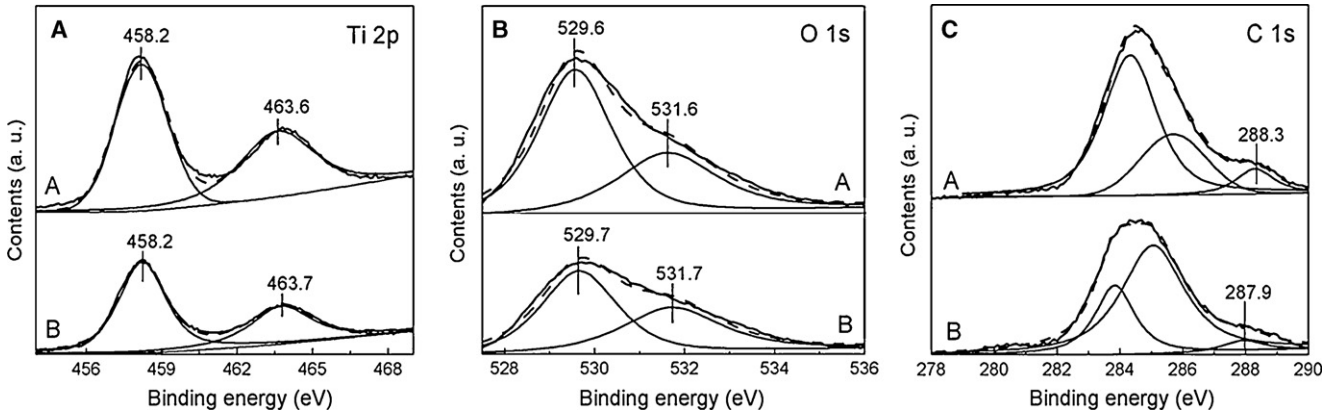

Fig. 9. XPS spectra of sample RH-80 (A) and PH104 (B): (a) Ti 2p, (b) O 1s and (c) C 1s.

3.2.3. Effect of acid in the formation of alkoxyl groups

Previously we stated the great effect of nitric acid in the synthetic process for the final visible-light activity. To search for the cause of this effect, we take samples PH100 and P100 for further investigation. From X-ray diffraction patterns (Fig. 11), we found that the peak height of anatase (1 0 1) plane for PH100 is much lower than that of P100; further investigation of other samples (SH-80, PH102 and P102, shown in Table 3) also revealed the selectively peak-height decrease on anatase (1 0 1) plane for samples synthesized with acid (SH-80, PH102). In the IR spectra of PH100 and P100 (inset of Fig. 11), the O–H stretching vibration of sample PH100 is much broader than that of P100, which indicates the richer amount of associated hydroxyl groups [37]. According to

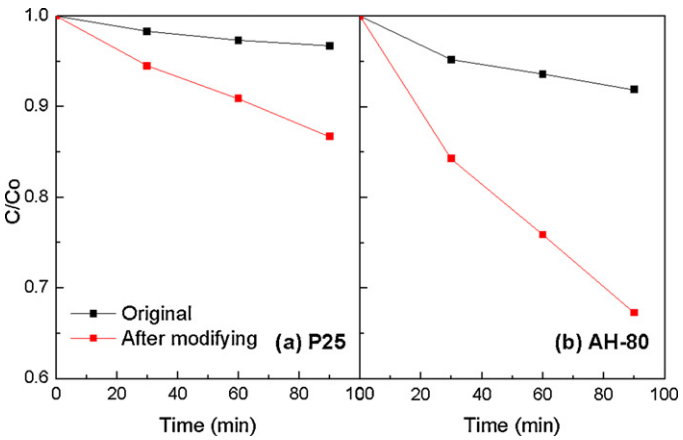

Fig. 10. MO degradation efficiency on TiO_2 samples (a) Degussa P25 and (b) AH-80 before and after modifying process.

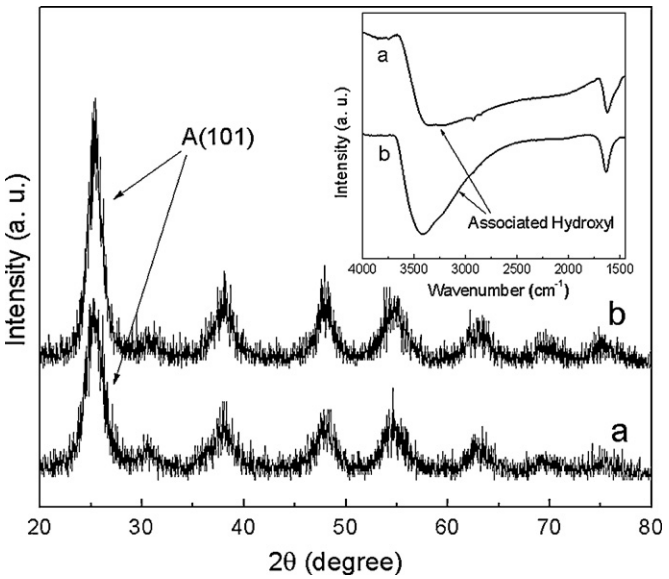

Fig. 11. XRD pattern and IR spectra (inset) of different TiO_2 samples (a) PH100 and (b) P100.

Table 3
Relative peak height of different TiO_2 samples in XRD patterns[a].

Sample	Plane				
	(1 0 1)	(0 0 4)	(2 0 0)	(2 1 1)	(2 0 4)
PH100	0.66	0.88	0.82	1.03	0.91
SH-80	0.72	0.93	0.84	1.04	1.05
PH102	0.71	0.84	0.82	0.99	0.94
P102	0.93	0.87	1.02	1.19	1.06

[a] The data shown in this table are relative to the peak height of sample P100 for each anatase plane.

these results, we assumed that in the refluxing process, the bridging oxygen atoms of the already-formed anatase (1 0 1) plane could be attacked by hydrogen ions sourced from the nitric acid; as a result, more hydroxyl groups were formed on the titania surface, and the further growth of anatase (1 0 1) plane was thus inhibited.

Diebold [38] has stated that the dissociation of alcohol caused by O–H bond scission would lead to adsorbed alkoxyl species and, probably, a hydroxylated oxygen atom; moreover, according to the research of Selloni et al. [39], there are favorable hydrogen bonding interactions with anatase (1 0 1) surface. Therefore, in our experiment, the adsorption of molecular or dissociative *n*-butanols could take place mainly on anatase (1 0 1) surface by H-bond interactions. Since the nitric acid could lead to enhanced formation of hydroxyl groups, it must be easier for the adsorbed *n*-butanols to be chemically linked on the titania surface. Fig. 12 shows a possible process of alkoxyl re-formation during refluxing: firstly, hydroxyl groups are formed mainly on anatase (1 0 1) surface; secondly, the nucleophilic butanol (or butoxyls) would attack the hydroxylated or unsaturated titanium ions by electrostatic forces, which results in the relaxation of Ti–OH bond; finally, combined with the attractive forces of adjacent hydrogen ions, some of the Ti–OH bonds are scissored and, simultaneously, some Ti–(O–Bu) covalent bonds are formed by the interactions between butoxyls and unsaturated titanium ions.

Moreover, from the C1s analysis (Fig. 9c) and the result of visible-light-activity measurement (Table 2), we observed that the RH-80 powder possessed not only more (Ti–O)–R bonds, but also better visible-light activity than PH104 (refluxed with more external *n*-butanols than RH-80). In fact, the photoactivities of sample PH101, PH102 and PH104 are similar, indicating the constrained process of ester bond re-formation during refluxing. Therefore, the presence of acid in Step 1 must have inhibited the hydrolytic process of TBT, which leads to more alkoxyl linkages. In a word, during the whole synthetic process of RH-80, there is a chemical equilibrium between the hydrolytic decomposition and re-combination of the Ti–(O–R) bond. The presence of acid and *n*-butanol cooperatively inhibits the hydrolytic process and promotes the re-combination process. Effective alkoxyl groups can either be the residues from incomplete hydrolysis of tetrabutyl titanate, or the –Ti–(O–R) groups re-formed in the refluxing process. Through sufficient stirring under atmospheric pressure, the method of refluxing provides an environment not only suitable for the further crystallization, but also favorable for the retention of superficial alkoxyl groups.

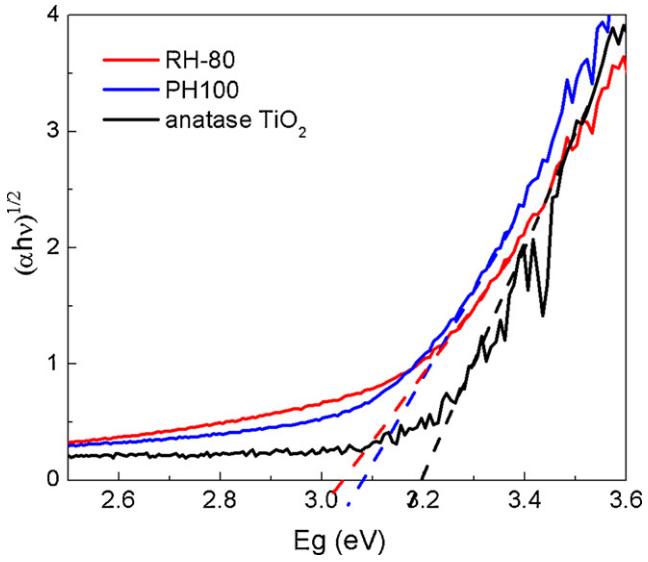

Fig. 13. Diffuse reflectance spectra of RH-80 and PH100 in comparison to the pure anatase.

3.3. Mechanism for the visible-light induced catalytic process

Fig. 13 shows the indirect band gap energies of sample RH-80 (C% = 0.730%), PH100 (C% = 0.313%) and pure anatase TiO_2 obtained in DRS characterization. From these curves we can see that the surface alkoxyl groups have slightly narrowed the band gap of anatase (3.04, 3.08 and 3.19 eV for sample RH-80, PH100 and pure TiO_2, respectively). However, the band gap of about 3 eV is simply too large to absorb photons with wavelength larger than 400 nm; in other words, the catalysts obtained in our experiments remain indirect semiconductors similar to the pure titania [40]. Emeline et al. have concluded that a surface photoreaction can be caused by the photoexcitation of both intrinsic and extrinsic absorption bands of a catalyst [41–44]. The former concerns with electron transitions from the valance band to conduction band, while the latter includes the photo-initialization of original or newly formed defects, the excitation of surface states, which could be realized by visible light. For our catalysts, the effect of superficial alkoxyl groups may be of the latter kind.

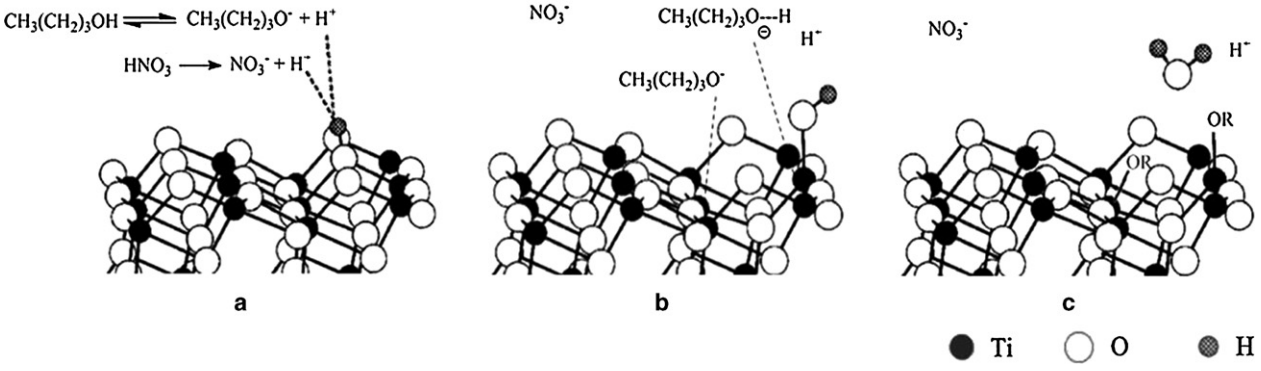

Fig. 12. Formation of alkoxyl groups during refluxing on anatase (1 0 1) surface: (a) adsorption of H^+ on bridging oxygen atoms, (b) hydroxylation of lattice oxygen and adsorption of butanols (or butoxyls) and (c) break of Ti–OH bond and formation of Ti–OR bond.

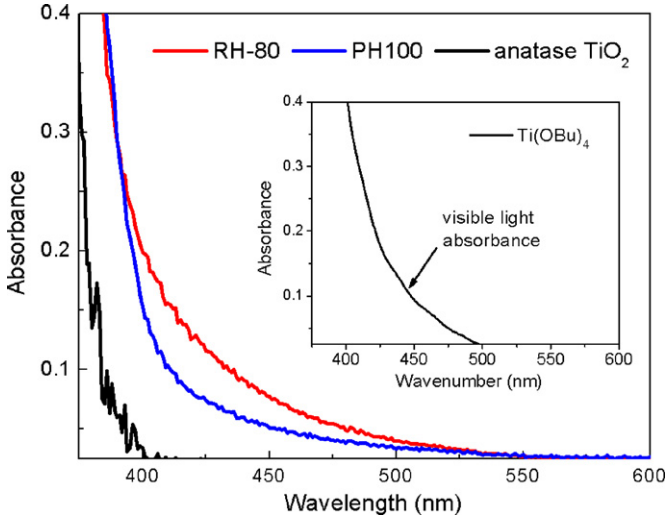

Fig. 14. Visible light absorption of RH-80 and PH100 in comparison to the pure anatase (inset: visible light absorbance of pure $Ti(OBu)_4$).

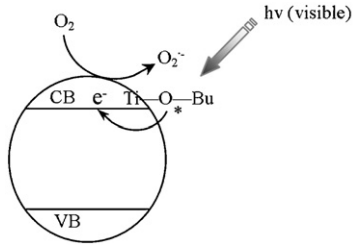

Scheme 1. Proposed visible-light-induced photocatalytic mechanism on alkoxyl-modified TiO_2 surface.

From the visible light absorption curves of sample RH-80, PH100 and anatase TiO_2 (obtained in DRS characterization), we found that the presence of surface alkoxyl groups has shifted the optical absorption of TiO_2 to visible light region (Fig. 14). Interestingly, the photo absorption behavior of RH-80 and PH100 are similar to the pure $Ti(OBu)_4$ (inset of Fig. 14), which is another evidence of the alkoxyl-derived visible light absorption. Some researchers [45,46] have proved that the complex formation between some colorless molecules and the surface of TiO_2 could lead to visible light absorption through a ligand-to-metal charge transfer (LMCT) process. In our case, the surface states in forms of Ti–O–R groups could also enable visible light excitation through electron transfer from the alkyl-linked oxygen (surface level) to the Ti (IV) site (conduction band). As is shown in Scheme 1, the photo-generated electrons could be trapped by the adsorbed oxygen to form highly active superoxides ($O_2^{\bullet -}$); and meanwhile, the excited ligands could also serve as oxidative sites for the degradation of targeted substrates. Therefore, it is understandable that the alkoxyl-derived surface modified TiO_2 possesses an effective visible-light activity.

4. Conclusions

The visible-light active anatase TiO_2 was prepared by controlled hydrolysis of tetrabutyl titanate in the nitric acid solution, followed with a refluxing process at 120 °C. Based on the results of various experiments and characterizations, we discovered that during the whole synthetic process, the presence of acid and hydrolysis products of TBT cooperatively lead to the formation of more alkoxyl groups on the anantase surface. The retained alkoxyls could induce visible light absorption through electron transfer from the alkyl-linked oxygen to the Ti (IV) site, so as to initiate the catalytic process. In consideration of crystalling method, the refluxing process at low temperature is very essential, because the effective alkoxyl groups were proved to be unstable under high temperature or hydrothermal conditions.

Acknowledgements

This work is financially supported by National Natural Science Foundation of China (No. 20907031). The authors are grateful to Ruibin Wang of the Instrumental Analysis Center of Shanghai Jiao Tong University for FTIR measurements, and Wenfeng Shangguan of School of Environmental Science and Engineering, Shanghai Jiao Tong University for DRS analysis.

References

[1] M.A. Fox, M.T. Dulay, Chem. Rev. 93 (1993) 341–351.
[2] M.I. Litter, Appl. Catal. B: Environ. 23 (1999) 89–114.
[3] M.R. Hoffmann, S.T. Martin, W. Choi, D.W. Bahnemann, Chem. Rev. 95 (1995) 69–96.
[4] N. Serpone, J. Phys. Chem. B 110 (2006) 24287–24293.
[5] W. Choi, A. Termin, M.R. Hoffmann, J. Phys. Chem. 98 (1994) 13669–13679.
[6] K. Nagaveni, M.S. Hegde, G. Madras, J. Phys. Chem. B 108 (2004) 20204–20212.
[7] J. Zhu, Z. Deng, F. Chen, J. Zhang, H. Chen, M. Anpo, J. Huang, L. Zhang, Appl. Catal. B 62 (2006) 329–335.
[8] J. Yin, X. Zhao, J. Phys. Chem. B 110 (2006) 12916–12925.
[9] A. Paola, G. Marci, L. Palmisano, M. Schiavello, K. Uosaki, S. Ikeda, B. Ohtani, J. Phys. Chem. B 106 (2002) 637–645.
[10] R. Asashi, T. Morikawa, T. Ohwakl, K. Aoki, Y. Taga, Science 293 (2001) 269–271.
[11] S.U.M. Khan, M. Al-Shahry, J. William, B. Ingler, Science 297 (2002) 2243–2245.
[12] H. Luo, T. Takata, Y. Lee, J. Zhao, K. Domen, Y. Yan, Chem. Mater. 16 (2004) 846–849.
[13] W. Zhao, W. Ma, C. Chen, J. Zhao, Z. Shuai, J. Am. Chem. Soc. 126 (2004) 4782–4783.
[14] X.T. Hong, Z.P. Wang, W.M. Cai, F. Lu, J. Zhang, Y.Z. Yang, N. Ma, Y.J. Liu, Chem. Mater. 17 (2005) 1548–1552.
[15] W. Ren, Z. Ai, F. Jia, L. Zhang, X. Fan, Z. Zou, Appl. Catal. B: Environ. 69 (2007) 138–144.
[16] D. Wu, M. Long, W. Cai, C. Chen, Y. Wu, J. Alloys Compd. 502 (2010) 289–294.
[17] H. Li, G. Zhao, Z. Chen, G. Han, B. Song, J. Colloid Interface Sci. 344 (2010) 247–250.
[18] J. Xu, Y. Ao, D. Fu, C. Yuan, J. Cryst. Growth 310 (2008) 4319–4324.
[19] J. Xu, Y. Ao, M. Chen, D. Fu, J. Alloys Compd. 484 (2009) 73–79.
[20] J. Xu, Y. Ao, D. Fu, C. Yuan, Appl. Surf. Sci. 254 (2008) 3033–3038.
[21] H.-Y. Hao, C.-X. He, B.-Z. Tian, J.-L. Zhang, Res. Chem. Intermediat. 35 (2009) 705–715.
[22] Z. Zhang, C.-C. Wang, R. Zakaria, J.Y. Ying, J. Phys. Chem. B 102 (1998) 10871–10878.
[23] P. Zabek, H. Kisch, J. Coord. Chem. 63 (2010) 2715–2726.
[24] C. Lettmann, K. Hildenbrand, H. Kisch, W. Macyk, W.F. Maier, Appl. Catal. B: Environ. 32 (2001) 215–227.
[25] C. Chen, M. Long, H. Zeng, W. Cai, B. Zhou, Mol. Catal. A: Chem. 314 (2009) 35–41.
[26] Y. Park, W. Kim, H. Park, T. Tachikawa, T. Majima, W. Choi, Appl. Catal. B: Environ. 91 (2009) 355–361.
[27] T. Bezrodna, G. Puchkovska, V. Shimanovska, I. Chashechnikova, T. Khalyavka, J. Baran, Appl. Surf. Sci. 214 (2003) 222–231.
[28] W.-C. Hung, S.-H. Fu, J.-J. Tseng, H. Chu, T.-H. Ko, Chemosphere 66 (2007) 2142–2151.
[29] D. Zhang, Y.R. Shen, G.A. Somorjai, Chem. Phys. Lett. 281 (1997) 394–400.
[30] P. Patino, N. Sanchez, H. Suhr, N. Hernandez, Plasma Chem. Plasma Process. 19 (1999) 241–254.
[31] M.K. Mamedov, E.K. Nabieva, R.A. Rasulova, Russ. J. Org. Chem. 41 (2005) 974–977.
[32] A.V. Stuart, G.B.B.M. Sutherland, J. Chem. Phys. 24 (1956) 559–570.
[33] H. Matsuura, H. Yoshida, M. Hieda, S.-Y. Yamanaka, T. Harada, K. Shin-ya, K. Ohno, J. Am. Chem. Soc. 125 (2003) 13910–13911.
[34] T. Kar, S. Scheiner, J. Phys. Chem. A 108 (2004) 9161–9168.
[35] A. Masunov, J.J. Dannenberg, J. Phys. Chem. A 105 (2001) 4737–4740.
[36] S. Sakthivel, H. Kisch, Angew. Chem. Int. Ed. 42 (2003) 4908–4911.
[37] P.M. Kumar, S. Badrinarayanan, M. Sastry, Thin Solid Films 358 (2000) 122–130.
[38] U. Diebold, Surf. Sci. Rep. 48 (2003) 53–229.
[39] A. Selloni, A. Vittadini, M. Gratzel, Surf. Sci. 402–404 (1998) 219–222.
[40] B. Neumann, P. Bogdanoff, H. Tributsch, S. Sakthivel, H. Kisch, J. Phys. Chem. B 109 (2005) 16579–16586.
[41] A.V. Emeline, K.R. Vladimir, N. Serpone, J. Phys. Chem. B 103 (1999) 1316–1324.
[42] A.V. Emeline, G.V. Kataeva, V.K. Ryabchuk, N. Serpone, J. Phys. Chem. B 103 (1999) 9190–9199.
[43] A.V. Emeline, G.N. Kuzmin, D. Purevdorj, V.K. Ryabchuk, N. Serpone, J. Phys. Chem. B 104 (2000) 2989–2999.
[44] A.M. Volodin, Catal. Taday 58 (2000) 103–114.
[45] F. Chen, W.W. Zou, W.W. Qu, J.L. Zhang, Catal. Commun. 10 (2009) 1510–1513.
[46] S. Kim, W. Choi, J. Phys. Chem. B 109 (2005) 5143–5149.